

# Shared Angles-of-Departure in Massive MIMO Channels: Correlation Analysis and Performance Impact

Xu Du, Ashutosh Sabharwal

**Abstract**—In practical environments, recent massive MIMO measurements demonstrate that user channels can be correlated. In this paper, we study the user channel correlation induced by shared angles-of-departure. We first derive the user correlation distribution in the large array regime, and then examine the user correlation using actual measurements from a large array. As a data-driven observation, we discover that the correlation of all close-by users is higher than 0.4 and barely reduces as the number of base-station antennas  $M$  increases beyond 36 antennas. Furthermore, nearly one-third of users, even when they are tens of wavelengths apart, have a correlation that is more than twice the correlation of an i.i.d. Rayleigh fading model. Lastly, we characterize the impact of user correlation on system performance. As  $M$  increases, conjugate beamforming systems suffer a linearly growing inter-user interference due to correlated channels. However, for zero-forcing beamforming systems, the inter-user interference is a constant that does not increase with  $M$ . In particular, zero-forcing beamforming systems can serve a linearly increasing number of correlated users and achieve a linear growth in the system achievable rate as  $M$  increases. Hence, spatial multiplexing correlated users can be an attractive massive MIMO design.

## I. INTRODUCTION

Massive multiple-input multiple-output (MIMO) is one of the key 5G components due to its potential benefits, including increased spectral efficiency [1], [2], wider coverage region [3], [4], [5], reduced channel variation [3], [4], and simplified physical layer precoding [1]. A commonly used model in the performance analysis of massive MIMO is the i.i.d. model, where the user channels become orthogonal as the number of base-station antennas increases. This mutual orthogonality is sometimes referred to as “favorable propagation” [6], [7], [5], [1], [2], [8].

As we move away from the assumption of favorable propagation, relatively less is known about the performance of massive MIMO. For i.i.d. Rayleigh fading channel, it is well-known that user channels are orthogonalized with a large number of base-station antennas. For spatial channels with various array configurations, past work [9], [10], [11] demonstrates that user channels are near orthogonal if the spatial paths are of independent angles-of-departure (AoDs) or the AoDs differences of spatial paths are larger than  $O(1/M)$ , where  $M$

is the base-station array size. Therefore, if the user channels consist of paths with distinct or independent AoDs, favorable propagation is likely to happen.

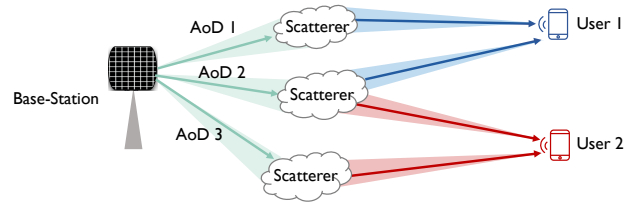


Fig. 1. An illustration of a two-user massive MIMO downlink channel with shared AoD. AoD 2 is shared by the two users and AoD 1, 3 are not shared by the two users. On the shared AoD 2, the two users’ AoDs with respect to the base-station are the same due to scatterer sharing. Note that the angles-of-arrival at the users are different. Later in Section III, we prove that User 1 and User 2 channels can be highly correlated even when the base-station has a large number of antennas.

However, in practical propagation environments, different users can share one or more paths with the same AoDs at the base-station. Fig. 1 depicts an example of two users sharing one common AoD due to scatterer sharing. Note that the angles-of-arrival at the users can be different in the AoD sharing paths. The sharing of common scatterers is known to happen more often when users are close-by. For example, the COST 2100 models [12], [13] introduced the “visible region” concept to capture the scatterer sharing of close-by users. The high correlation of close-by users is also confirmed by recent massive MIMO measurements [14], [15], [16], [17], [18]. Additionally, practical propagation environments might contain keyholes [3, Chapter 7.3], which lead to shared AoDs for even far-away users. Finally, in a practical deployment setting, the array configuration [19] can limit the user channel orthogonality. For example, for an array with a limited horizontal aperture, the spatial resolution of azimuth is limited. Therefore, two paths with a similar elevation AoD but a small azimuth AoD difference cannot be distinguished by adding more antennas on the vertical domain.

If we accept the existence of shared AoDs, the user channels cannot be viewed as independently distributed and can be of high correlation. It might seem natural for a massive MIMO base-station to avoid spatial multiplexing correlated users [3], [11], [20], as user correlation can reduce the effective SINR in beamforming. However, not spatial multiplexing correlated users can be sub-optimal. For example, spatial multiplexing many slightly correlated users often leads to higher system

Xu Du is with Facebook Inc., Hacker 1 Way, Menlo Park, CA, 94025. Ashutosh Sabharwal is with the Department of Electrical and Computer Engineering, Rice University, Houston, TX, 77005 (e-mails: xdurice@gmail.com, ashu@rice.edu). This work was conducted when Xu Du was with Rice University, Houston, Texas, 77005. This work was partially supported by NSF grants CNS-1518916 and CNS-1827940, and a grant from Qualcomm, Inc.

achievable rate than spatial multiplexing a few non-correlated users. Another example is that if all users are correlated due to the keyhole effect, spatial multiplexing correlated users can result in a higher system achievable rate than just beamforming to one user. Thus, to design massive MIMO systems for their intended use, a key question is *how does the achievable rate and the optimal degree of spatial multiplexing change with user correlation?*

We answer this question by accepting the fact that different users may have one or more paths of the same AoDs. We characterize the impact of such shared AoDs via a combination of theoretical analysis and experiments. Our main contributions are as follows:

- 1) We first adopt a spatial geometric channel model to compute the user correlation when shared AoDs exist. In the large array regime, the user correlation of two users is shown to converge to a random variable that is independent of the number of base-station antennas  $M$ . As  $M$  increases, the mean of the square of user correlation converges to a positive value that is proportional to the sum of the gains of the AoD sharing paths.
- 2) To examine user correlation over-the-air, we collect a diverse massive MIMO channel data set with a 64-antenna planar array. Our evaluation includes both line-of-sight (LOS) and non-line-of-sight (NLOS) propagation environments with more than 11000 unique user channel vectors from 225 different locations. The measured channels are now open-accessed at [21]. With a 64-antenna base-station array, the channel correlation between *all* close-by users is higher than 0.4. In our data set, the user correlation of close-by users reduces very slowly when the number of base-station antennas  $M$  is larger than 36. For users that are far-away, we find that the correlation of more than 28.6% users is at least twice the correlation of i.i.d. Rayleigh fading. The observed user correlation is near-constant across the 20 MHz measured band. Finally, we use spatial signal processing to confirm that shared AoDs are the root cause of high correlation for both close-by and far-away users.
- 3) To understand the system performance impact of user correlation, we characterize the effective SINR of massive MIMO with both user and base-station array correlation. The base-station adopts conjugate beamforming or zero-forcing beamforming to serve *correlated* users. For conjugate beamforming systems, spatial multiplexing correlated users introduces inter-user interference that increases linearly with  $M$  due to user correlation. For zero-forcing beamforming systems, however, spatial multiplexing correlated users only results in a SINR loss factor that does not increase with  $M$ . As a result, zero-forcing beamforming systems can serve a linearly growing number of users while maintaining the same SINR as  $M$  increases. We further utilize measured channels to demonstrate that zero-forcing based systems can support a linearly growing number of correlated users. Therefore, user correlation itself does not limit

the multiplexing gain of massive MIMO. And a proper beamforming design can help mitigate the user correlation and make spatial multiplexing correlated users attractive.

*Related Work:* One of the early measurement work [22] first demonstrated that the average far-away user correlation reduces as the number of base-station antennas increases. By measuring tens of close-by user channels with uniform linear array [14], [15], uniform cylindrical array [14], [18], uniform rectangular planar array [16], [17], recent channel measurements find that channels of close-by users can have high correlation. Our measurements follows the same stream of past experimental work. We measured and open-accessed user channels at 225 unique locations in both LOS and NLOS environments with a 64-antenna calibrated array. During our measurements, we observed high user correlation not only for close-by users, but also for 28.6% of the far-away users. Using spatial signal processing, we confirm that the shared AoDs are the root cause of high user correlation for both close-by and far-away users.

The performance of massive MIMO is usually evaluated in either i.i.d. Rayleigh fading channel [6], [7], [5], [1], [2], [8], [23], [24] or massive MIMO channel with base-station array correlation [25], [26], [27], [4], [28], [29], [30], [31]. The reference in a recent review paper [32] provides more details. In the evaluation of massive MIMO with base-station array correlation, the channel vector of each user is usually considered *independently distributed* complex Gaussian variables with a similar or different covariance matrix. As a result, any two user channels are near orthogonal under the past evaluations, and correlation among users is not captured. A special case of two users downlink with limited user correlation and zero-forcing beamforming has been studied in [33]. A recent work [20] characterizes the massive MIMO performance in line-of-sight propagation environments. With the proposed simple user dropping algorithm, [20] demonstrates that massive MIMO can have comparable performance to i.i.d. Rayleigh fading if the line-of-sight path AoDs is independently distributed across users. This paper generalizes the past work to characterize a  $K$ -user massive MIMO system under arbitrary user correlation, i.e., cases when users can share AoDs. We note that some past research, including [31], refers to the limited (or fixed) user channel covariance matrix rank due to scattering sparsity as “spatial correlation”. However, [31] still considers the user channel realizations to be independent. Hence, the “spatial correlation” in [31] is fundamentally different to the characterized user correlation in this paper.

The paper is organized as follows. We first describe the system model in Section II. Section III derives the user correlation of users with shared AoDs. We present a channel measurement campaign and characterize the user correlation over-the-air in Section IV. We quantify the system performance impact of user correlation in Section V. Numerical simulation is used to verify the analytical results in Section VI. Finally, Section VII concludes the main findings of this paper.

*Notations:* Boldface represents vectors and matrices. We use  $|\cdot|$  to denote the magnitude of a complex number. And the  $l_2$ -norm of a complex vector is  $\|\cdot\|$ . The space

of the real number is  $\mathbb{R}$  and  $\mathbb{C}$  is the complex space. The complex Gaussian and complex matrix Gaussian distributions are denoted by  $\mathcal{CN}$  and  $\mathcal{CMN}$ , respectively. The Kronecker product and matrix vectorization operations are denoted by  $\otimes$  and  $\text{vec}(\cdot)$ , respectively. The conjugate transpose and trace of a matrix  $\mathbf{H}$  are denoted as  $\mathbf{H}^H$  and  $\text{tr}\mathbf{H}$ , respectively. An  $M \times M$  identity matrix is  $\mathbf{I}_M$ . And diagonal matrix is  $\text{diag}(\cdot)$ . Finally, an  $M$ -element all-ones (all-zeros) vector is  $\mathbf{1}_M$  ( $\mathbf{0}_M$ ) and a  $K \times M$  all-ones (all-zeros) matrix is  $\mathbf{1}_{K \times M}$  ( $\mathbf{0}_{K \times M}$ ).

## II. SYSTEM MODEL

We consider a single-cell massive MIMO downlink system with an  $M$ -antenna base-station and  $K$  single-antenna mobile users. We assume that the base-station is time synchronized with the  $K$  users. The downlink channel is  $\mathbf{G}\mathbf{H}$ , where  $\mathbf{G} = \text{diag}(\sqrt{\gamma_1}, \sqrt{\gamma_2}, \dots, \sqrt{\gamma_K})$  is the large-scale channel gains and  $\mathbf{H} \in \mathbb{C}^{K \times M}$  denotes the small-scale fading. The base-station adopts downlink beamforming to serve all  $K$  users at the same time. Let the downlink beamforming matrix be  $\mathbf{V} \in \mathbb{C}^{M \times K}$ . The received signals by users then equal

$$\mathbf{y} = \mathbf{G}\mathbf{H}\mathbf{V}\mathbf{s} + \mathbf{w}, \quad (1)$$

where  $\mathbf{w} \in \mathbb{C}^K$  is the additive noise, whose elements follow standard complex Gaussian distribution. Following the convention [3], we assume that the signal sequence  $\mathbf{s}$  follow standard complex Gaussian distribution, i.e.,  $E[\mathbf{s}] = \mathbf{0}$  and  $E[\|\mathbf{s}\|^2] = 1$ . The total transmission power is  $P$ , which equals  $E[\text{tr}\mathbf{V}\mathbf{V}^H]$ . Prior to the data transmission, the base-station estimates the downlink channel  $\hat{\mathbf{H}} \in \mathbb{C}^{K \times M}$  for beamforming.

In Section III and Section IV, we will utilize theoretical analysis and measurements to characterize the user correlation of downlink channel  $\mathbf{H}$ . In Section V, we will derive the effective SINR for massive MIMO with both user and base-station correlation.

## III. MODELING USER CORRELATION: A SPATIAL PERSPECTIVE

In this section, we characterize the impact of shared AoDs by considering a generalized spatial geometric model, where users can share AoDs due to scattering sharing. The spatial geometric models have been widely adopted to model propagation environments in both standardizations [34] and research [13], [9], [3], [4], [35].

### A. User Correlation Definition

The orthogonality of user channels is often measured by the cosine similarity, i.e., correlation of the downlink channel vectors. The correlation of User  $k_1$  and User  $k_2$  equals

$$c(\mathbf{h}_{k_1}, \mathbf{h}_{k_2}) = \frac{|\mathbf{h}_{k_1}^H \mathbf{h}_{k_2}|}{\|\mathbf{h}_{k_1}\| \|\mathbf{h}_{k_2}\|}. \quad (2)$$

In past massive MIMO literature [6], [7], [5], [1], [2], [8], the desired pairwise channel orthogonality is usually referred to as *favorable propagation*, which is defined as

$$c(\mathbf{h}_{k_1}, \mathbf{h}_{k_2}) = 0, \text{ for all } k_1 \neq k_2, k_1, k_2 = 1, 2, \dots, K. \quad (3)$$

Therefore, a propagation environment is considered “favorable” if all user pair channels are mutually orthogonal. In practical systems with a finite number of antennas, Condition (3) is always not satisfied. However, Condition (3) might be approximately satisfied in the large array asymptotic regime. We define such case as *asymptotically favorable propagation*, which is

$$\lim_{M \rightarrow \infty} c(\mathbf{h}_{k_1}, \mathbf{h}_{k_2}) = 0, \text{ for all } k_1 \neq k_2, k_1, k_2 = 1, 2, \dots, K. \quad (4)$$

In this section, we want to find if and under what condition would (4) be satisfied. Furthermore, we are interested in characterizing how far a practical massive MIMO system can be away from condition (4). Without loss of generality, we focus on computing the correlation between two users whose channels are denoted by  $\mathbf{h}_1$  and  $\mathbf{h}_2$ .

### B. Spatial Channel Model

A spatial geometric channel model describes the channel vector by modeling spatial paths. The considered channel model is illustrated in Fig. 1. The base-station is equipped with a two-dimensional uniform planar antenna array on the  $xy$ -plane. In total, there are  $L$  AoDs from the base-station to the two users.

The base-station is equipped with an  $M$ -antenna uniformly spaced planar array. There are  $M_x$  antennas on the  $x$ -axis, and  $M_y$  antennas on the  $y$ -axis. Let  $(\theta_x^l, \theta_y^l)$  be the  $l$ -th elevation and azimuth AoD. For a typical cellular network, the base-station is elevated high above the ground and free from local scatterers. Therefore, the base-station is in the far-field and the channel of User  $k$  equals

$$\mathbf{h}_k = \sum_{l=1}^L \sqrt{g_k^l} e^{j\phi_k^l} \mathbf{a}(\theta_x^l, \theta_y^l), \quad (5)$$

where path gain and phase of Path  $l$  of User  $k$  are  $0 \leq g_k^l < 1$  and  $\phi_k^l$ , respectively. Here,  $\mathbf{a}(\theta_x^l, \theta_y^l)$  is the array response vector for a plane wave at direction  $(\theta_x, \theta_y)$ , which equals [4, Chapter 7]

$$\mathbf{a}(\theta_x, \theta_y) = [1, e^{j\Delta 2\pi \sin \theta_y \cos \theta_x}, \dots, e^{j\Delta 2\pi \sin \theta_y [(M_x - 1) \cos \theta_x + (M_y - 1) \sin \theta_x]}], \quad (6)$$

where  $\Delta$  is the ratio between the antenna spacing and the wavelength of the carrier frequency. It is noted that the spatial angles  $(\theta_x^l, \theta_y^l)$  are with respect to the base-station array plane. For User  $k$ , if there is no path gain from base-station in AoD  $l$ , then  $g_k^l$  equals 0.

By channel model in (5), the distribution of each user channel is determined by the gain, phase, and AoD of the  $L$  paths. Thus, the joint distribution of the path parameters for the two users further determines the distribution of user correlation. To facilitate the user correlation analysis, we make the following assumptions on the distribution of the channel parameters:

- *Random path phases:*  $\phi_k^l \sim U[0, 2\pi]$ .
- *Random angles:*  $\theta_x^l \sim U[0, 2\pi]$ , and  $\theta_y^l \sim U[0, \pi]$ , for all  $l$ .

- *Non-trivial 2D planar array:* As  $M$  increases, the  $M_x$  and  $M_y$  both increase at a fixed ratio.

Firstly, the phase of each path follows an independent uniform random distribution between 0 and  $2\pi$ . The random phase assumption is justified by considering that the distances traveled by the paths are much larger than the wavelength at the carrier frequency. Additionally, the AoDs follow independent uniform distributions in both elevation and azimuth. And the path gains can be any non-negative scalars.

The spatial model (5) can capture user paths of independent AoDs and shared AoDs. For example, if  $g_1^l g_2^l = 0$  for all  $l$ , there is no shared AoDs and the AoDs is independent for the two users. If  $g_1^l g_2^l > 0$ , User 1 and User 2 channels both contain contributions from AoD  $l$ , i.e., AoD  $l$  is shared. During our analysis, we compute the user correlation by treating  $g_1^l$  and  $g_2^l$  as constants. In Section III-D, we will discuss the implications of the analysis by considering different combinations of  $g_1^l$  and  $g_2^l$ .

### C. User Correlation Analysis

With the spatial channel model in (5), we now characterize the user correlation in the large array regime. We first demonstrate that the user correlation does not necessarily diminish to zero if shared AoDs happen. Instead, as the number of base-station antennas  $M \rightarrow \infty$ , the user correlation converges in distribution to a non-trivial random variable that is independent of  $M$ .

**Theorem 1** (Convergence of User correlation). *The user correlation converges in distribution to a random variable that is independent of the number of base-station antennas as*

$$\lim_{M \rightarrow \infty} c(\mathbf{h}_1, \mathbf{h}_2) \xrightarrow{d} \left| \sum_{l=1}^L \sqrt{\frac{g_1^l}{\sum_{l=1}^L g_1^l} \frac{g_2^l}{\sum_{l=1}^L g_2^l}} e^{j\tilde{\phi}^l} \right|. \quad (7)$$

Here,  $\tilde{\phi}^l$  is a random variable that is uniform between 0 and  $2\pi$ .

To prove the theorem, the key step is to demonstrate that a normalized product between two paths with independently random AoDs converges to zero. We provide detailed proof in Appendix VIII-A. Theorem 1 shows that the asymptotic correlation converges to the amplitude of the resulting field of a ‘‘random-walk problem’’ [36] on the complex plane. Each ‘‘random-walk’’ step is of uniform random phase with a step size of  $\frac{g_1^l}{\sum_{l=1}^L g_1^l} \frac{g_2^l}{\sum_{l=1}^L g_2^l}$ . Recall that if AoD  $l$  is shared, then  $g_1^l g_2^l > 0$ . Therefore, when the number of AoDs is finite, the asymptotic user correlation would not diminish with shared AoDs. To provide insights into the structure of user correlation, we now characterize its asymptotic mean and variance.

**Corollary 1** (Equivalence of User Correlation and Shared Path Gain). *In the large array regime, the mean and variance of the square of the user correlation both converge to fixed points. The mean is given by*

$$\lim_{M \rightarrow \infty} E[c^2(\mathbf{h}_1, \mathbf{h}_2)] = \sum_{l=1}^L \frac{g_1^l}{\sum_{l=1}^L g_1^l} \frac{g_2^l}{\sum_{l=1}^L g_2^l}, \quad (8)$$

and the variance satisfies

$$\lim_{M \rightarrow \infty} \text{Var}[c^2(\mathbf{h}_1, \mathbf{h}_2)] = \frac{\sum_{l_1=1}^L \sum_{l_2=1, l_2 \neq l_1}^L g_1^{l_1} g_2^{l_1} g_1^{l_2} g_2^{l_2}}{\left( \sum_{l=1}^L g_1^l \sum_{l=1}^L g_2^l \right)^2}. \quad (9)$$

The proof is immediate by characterizing the random variable that user correlation converges to; Appendix VIII-B provides the proof details. Since  $\sum_{l=1}^L g_k^l$  is the total downlink path gain,  $\frac{g_k^l}{\sum_{l=1}^L g_k^l}$  denotes the path gain proportion of AoD  $l$ . Therefore, Corollary 1 shows that the expectation converges to sum of the path gain products of AoD sharing paths.

As a result of shared AoDs, two users that receive the dominant energy from the same set of scatterers are correlated even when the array size is large. With a finite  $L$ , the user correlation converges to 0 if and only if *no* path share AoD, i.e.,  $g_1^l g_2^l = 0$ , for all  $l$ . Recall that no path share AoD in (5) is equivalent to users with independent AoDs. Therefore, past user correlation analysis on users with independent AoDs [9], [10], [11] can be viewed as a special case of our analysis. We note that Corollary 1 can also be proved alternatively by computing the channel covariance matrix under channel model in Section III-B, and substituting the covariance matrix into [4, (2.19)].

### D. User Correlation with Small AoDs difference

Section III-C characterizes the user correlation when users share the same AoDs from common scatterers. In reality, it is possible that for a shared scatterer, the AoDs can have small differences among users. To understand the impact of such AoDs difference, we now conduct numerical experiments. During the numerical experiments, we follow the channel model in Section III-B, but make the AoDs (to the same scatter) of different users have an AoD difference. The AoD difference is modeled by a 2-D complex Gaussian variable with zero mean and variance of  $\delta^2$ , where  $\delta$  is the standard deviation of the AoD difference in both elevation and azimuth.

Fig. 2 (left) presents the mean of the square of the user correlation obtained by numerical simulations ( $\delta = 1^\circ$ ) and Corollary 1. Even with a small AoD difference, the user channels can still be of high correlation when the number of base-station antenna is larger than 160. The numerical simulation also confirms Corollary 1 on that user correlation reduces with the shared path gains.

Fig. 2 (right) presents the theoretical predictions and numerical simulations for two users with equal power gain across varying number of paths, and different level of user AoD differences. As expected, the user correlation reduces with the number of paths and the AoD difference. In practical propagation environments, the number of paths is limited [34]. And we expect users with shared AoDs to be of potentially high correlation.

## IV. MEASURED USER CORRELATIONS

In this section, we examine user channel correlation based on over-the-air measured channels. The collected channel data set is also open-accessed for download at [21].

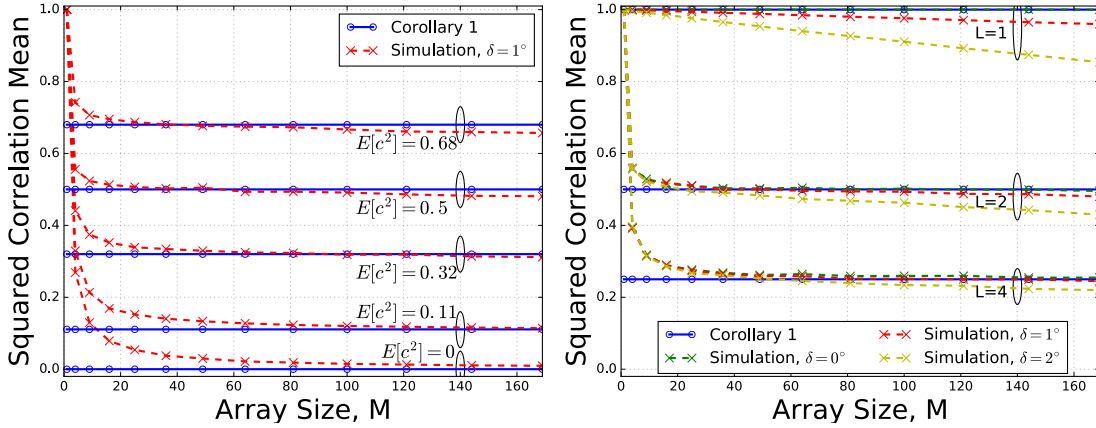


Fig. 2. User correlations with shared AoDs in channel model (5). The elevation and azimuth AoD difference of each shared scatterer between the two users are modeled by i.i.d. Gaussian random variables with a standard deviation of  $\delta$ . Figure left demonstrates that user channel correlation increases with the gain of AoD sharing paths. Figure right demonstrates that user channel correlation reduces with multipath and AoD difference. Both figures demonstrate that user correlation can be high even when the number of base-station antennas is  $> 160$ . Here, we call the square of user correlation as squared user correlation for shorthand. In the simulation, square planar arrays with half-wavelength spacing are used, i.e.,  $M_x = M_y$  and  $\Delta = 0.5$ . In the left figure, there are 2 AoDs with different path gains. Each red dashed line corresponds to a different path gain combination. From the low gain in the shared AoDs to the high gain in the shared AoDs, the path gain combinations used are  $[(0, 1), (1, 0)]$ ,  $[(0.0625, 1), (1, 0.0625)]$ ,  $[(0.25, 1), (1, 0.25)]$ ,  $[(1, 1), (1, 1)]$ ,  $[(1, 0.25), (1, 0.25)]$ . In the right figure, two users share all  $L$  paths with a same path gain.

## A. Measurement Setup

1) *Measurement Platform*: We measure the OTA channels on the campus of Rice University near the Anne and Charles Duncan Hall (N 29.720138°, W 95.39876°). The channels were measured by using a massive MIMO base-station (developed as part of the Argos project [37]) and mobile clients. The users are in a near stationary environment. The measurements are on the 2.4 GHz Wi-Fi ISM band with 20 MHz bandwidth. Both the base-station and users are equipped with patch antennas with 3-dB beam-width of around 120-degree. The  $8 \times 8$  64-antenna array and a mobile user are shown in Figure 3.

2) *Measured Locations*: The channel between the base-station antennas and users from 4 line-of-sight (LOS) clusters and 5 non-line-of-sight (NLOS) clusters are measured. Each cluster is of circle-shape with a diameter of around 4 meters. Figure 3 presents the locations of the massive MIMO station and user clusters. In each cluster, we measure the user channels of 25 *different* uniformly selected locations. Therefore, the minimum distance between two users from the same cluster is about 0.7 meters. In total, we measure the mobile user channels in 225 locations. For each location, we measure the uplink channel between a mobile user and the base-station of the 52 non-empty subcarriers over the 20 MHz band in more than 140 frames. In our evaluations, we will utilize all subcarriers from the first frame of each location. In total, we characterize the user correlation over-the-air based on more than 11000 unique channel vectors.

3) *Array Calibration for Antenna Phase Mismatch*: For the Argos [37] massive MIMO base-station, each antenna is connected to an individual radio-frequency chain. During channel measurements, each base-station antenna estimates its channel coefficient by correlates the received signal with an uplink pilot sequence. As the phase-locked loop component of each radio-frequency chain introduces an independent ran-

dom phase to each antenna, the collected channel contains mismatched phases across different base-station antennas and different measured locations. Such phase mismatch raises two critical issues in the examination of user correlation. Firstly, the phase mismatch across base-station antennas makes the (uplink) angle-of-arrival estimation infeasible. The reason is that the angle-of-arrival estimation requires a phase synchronized array [39]. Secondly, phase mismatches across different measurements obstruct the user correlation computation of channels measured at different locations. The challenges comes from that the correlation computation (2) requires that each base-station antenna have a fixed (relative) phase offset during measurements of different users. Thus, array calibration of the phase mismatch is essential for both the angle estimation and the user correlation computation.

To calibrate the phase mismatch, we introduce a calibration node in all measurements. The calibration node is placed perpendicular to the array plane at the direction of elevation angle  $0^\circ$  and azimuth  $0^\circ$ . The distance between the calibration node and the base-station array is about 20 meters. The main path is at  $(0^\circ, 0^\circ)$ . Fig. 3 shows that there might exist an addition ground reflection path, which is about  $4.6^\circ$  elevation away from the main path. Since the ground reflection path should be of much lower gain and the angle difference is small, the channel between the calibration node and the array can be modeled as  $\mathbf{a}(0^\circ, 0^\circ) = \mathbf{1}_M$ . Therefore, by measuring the uplink channel from the calibration node to the base-station, we obtain the relative phase mismatch of each base-station antenna. To determine the calibrated channel of each location, we measure the channels of both the mobile and the calibration node in *all* channel measurements. The calibrated channel of each location is then obtained by element-wise division of the mobile node channel over the calibrate node channel.



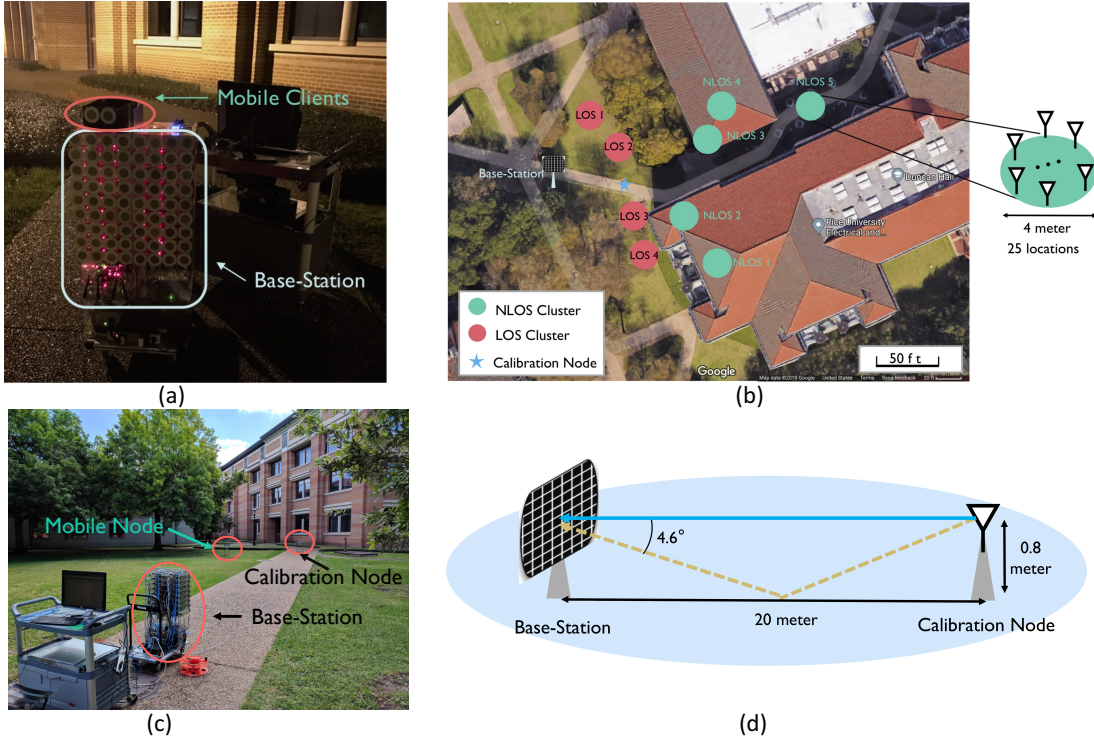


Fig. 3. Argos [37] Massive MIMO base-station and the over-the-air measurements setup. The background map of the top right figure is from Google Maps [38].

### B. Experimental User Correlation Examination

We want to characterize the distribution of the user correlation as a function of the user geolocational separation and the number of paths. Primarily, we are interested in finding how often does the high user correlation happen. In evaluations, when computing channel correlation for  $M < 64$ , we subsample square sub-arrays of dimension  $\sqrt{M} \times \sqrt{M}$ . For example, when  $M = 36$ , all antennas from the first 6 rows and first 6 columns are selected. In all channel measurements, the measured channel SNR of each antenna is over 15 dB. We hence compute the channel correlations by treating the measured channels as perfect.

*Finding 1 – Close-by User Channels Correlation Decays Very Slowly When  $M > 36$ :* We first evaluate the user channel correlation between close-by users from the same cluster, i.e., *intra-cluster correlation*. Fig. 4 presents the computed intra-cluster correlation of the 9 clusters whose locations are described in Fig. 3. Each data point on each curve is obtained by averaging over 15600 unique channel pairs among the 25 locations in the 52 subcarriers. And the error bar represents the variation of intra-cluster across the 52 different subcarriers. The average user channel correlation under i.i.d. Rayleigh fading is also presented as a benchmark. For user channels measured in LOS clusters, intra-cluster correlation reduces very slowly as  $M$  increases. Over the measurements, we observed intra-cluster user channels correlation over 0.8 for *all* LOS clusters even when the base-station is equipped with 64 antennas. For NLOS clusters, intra-cluster correlation reduces quickly when  $M$  is smaller than 25. When  $M > 36$ , the intra-cluster correlation of NLOS clusters reduces very slowly or does not decrease. And NLOS environments, in general, lead

to lower intra-cluster channel correlation than that of LOS environments. The lower intra-cluster correlation in NLOS environments can be explained by the multipath effect and matches with Observation 2 in Section III-D.

In summary, for *all* clusters, an intra-cluster channel correlation of more than 0.4 is observed with the 64-antenna array. It is noted that the measured high intra-cluster correlations agrees with past measurements of close-by users [14], [15], [16], [17], [18].

*Finding 2: Far-away Users Decorrelate Statistically Not Globally:* We next shift our attention to the channel correlation between users from different clusters, or *inter-cluster correlation*. We first review the statistical average of the correlation between the 25 users from each cluster to all other 200 users from the other clusters across the 52 subcarriers. Fig. 4 provides the calculation results, and each point of every curve is acquired by averaging over 260000 unique channel pairs. The error bars show the standard deviation across the 52 subcarriers. Unlike intra-cluster correlation, the inter-cluster correlation does reduce as the number of base-station antennas  $M$  increases, which agrees with past measurement of far-away users [22]. We remark that the statistical average of the inter-cluster channel correlation can be higher than that over i.i.d. Rayleigh fading.

To understand the slow correlation decay of the statistical average, we now examine the mean and standard deviation of the channel correlation between users from any pair of clusters in Figure 5. Each grid of the matrix denotes the average channel correlation of a different cluster pair. The diagonal elements denote the intra-cluster channel correlation (each averaged over 15600 channel vector pairs). And the off-

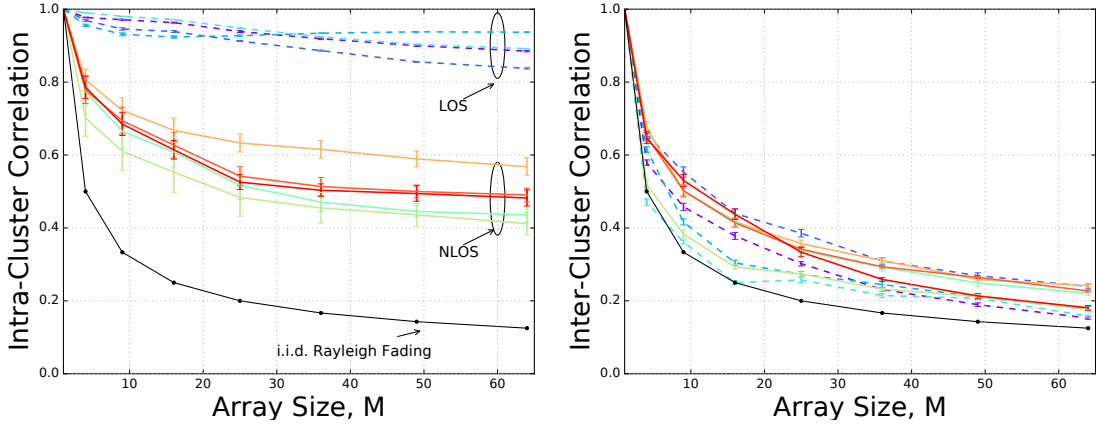


Fig. 4. Measured user channel correlation. Figure on the left (right) represents the computed user correlation of measured channels from the same (different) clusters. Each computed intra-cluster and inter-cluster user channel correlation comes with the standard error bar. The error bars denote the correlation variation across the 52 subcarriers. The two sub-figures share the same legend. The solid black line is for i.i.d. Rayleigh fading. The solid and dashed colored lines are for NLOS and LOS clusters, respectively.

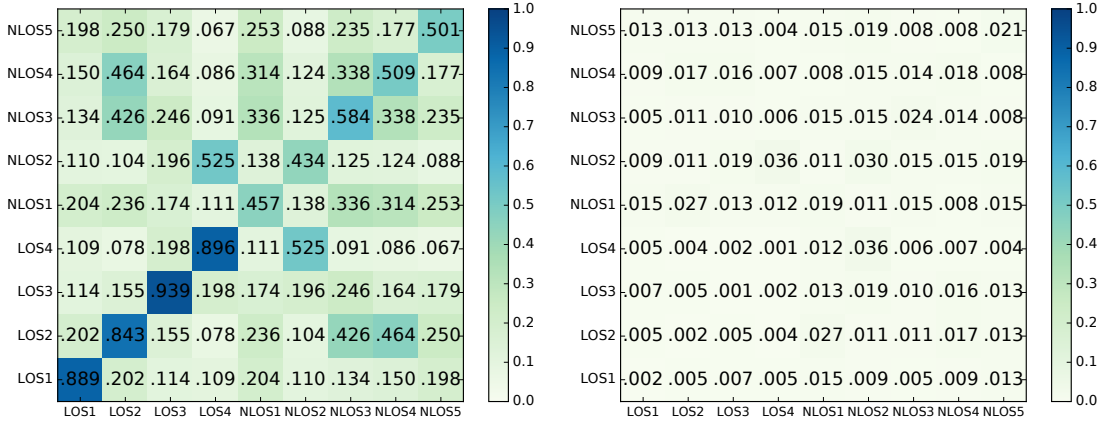


Fig. 5. User correlation mean and standard deviation of measured channels. Here,  $M = 64$  and each grid is the mean and standard deviation of user correlations between all pairs of clusters. Each grid is the user channel correlation average or standard deviation between a cluster labeled by the  $x$ -axis and a cluster labeled by  $y$ -axis.

diagonal elements denote the channel correlation of users from different clusters (each averaged over 32500 channel vector pairs). Interestingly, we find that the inter-cluster correlation of some cluster pairs is still significant even with an array size of 64. For example, between Cluster LOS 4 and Cluster NLOS 2, the inter-cluster correlation is 0.522. And 28.6% of the 28 cluster pairs have inter-cluster correlation at least twice of that in i.i.d. Rayleigh fading. In summary, the statistical average of far-away user correlation reduces as the array size increases. However, some far-away user pairs can still be of high correlation even with a 64 antenna array.

#### Finding 3 – High User Correlation Caused by Shared AoDs:

The theoretical analysis in Section III proves that shared AoDs lead to a significant correlation. To verify that the shared AoDs are the root causes for over-the-air user correlation, we present spatial angle estimation examples of the measured channels. We first consider the intra-cluster correlation. Fig. 6 and 6 present the estimated angle energy heat map of two different locations of NLOS 2. We find that the two locations share common angles near  $(28^\circ, 0^\circ)$  and  $(15^\circ, 15^\circ)$ . The shared up-link angles-of-arrival (downlink angles-of-departure) explain

the observed 0.434 intra-cluster correlation when  $M = 64$  in NLOS 2.

Furthermore, we confirm that shared AoDs are also the root causes of far-away but correlated users. For example, users from NLOS 2 is of correlation 0.525 with users from LOS 4, which can be directly verified by the common angle estimated in Fig. 6. To provide an example of user channels quickly orthogonalize as array size increases, we consider the inter-clusters correlation between NLOS 3 and NLOS 2, which is 0.125 with 64 antennas. Fig. 6 shows the estimated angles for a location in NLOS 3. Thus, the distinct spatial angles of NLOS 3 and NLOS 2 explain the low user correlation.

#### Finding 4 – User Correlation Near Constant Across the Frequency Band:

Finally, we want to profile user correlation variance over different frequency subcarriers. The error bars in Fig. 4 denote the variation of the intra-cluster and inter-cluster correlations across the 52 subcarriers. Each grid in Fig. 5 presents the standard deviation of the average user correlation among the 52 subcarriers. The small error bars in Fig. 4 and small standard deviation values in Fig. 5 hence demonstrate that the intra-cluster and inter-cluster correlation

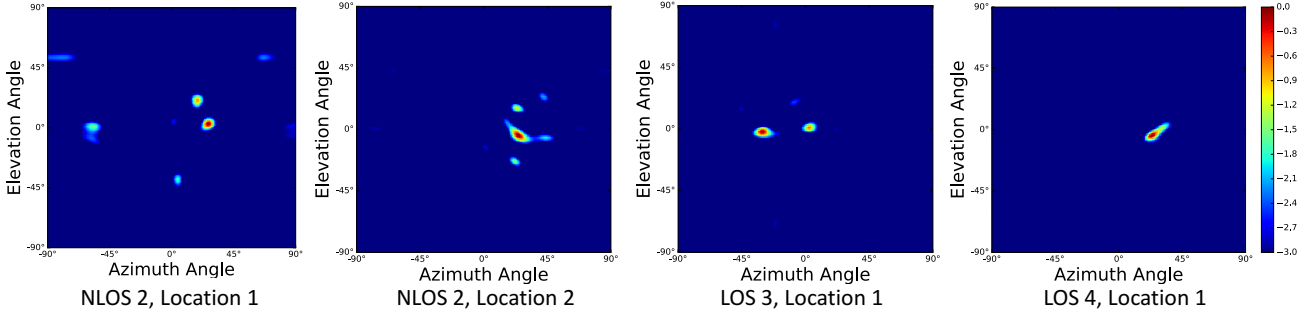


Fig. 6. The estimated power angle map of measured user channels via MUSIC [39]. Each point of each figure approximates the logarithmic energy of each direction.

is near constant across the 20 MHz band.

In this section, we confirm that the shared AoDs are the root causes behind high user correlation in practical propagation environments. In our data set, the high user correlation of close-by users barely reduces when  $M > 36$ . For 28.6% of far-away user pairs, the shared AoDs result in a correlation that is more than twice the correlation in i.i.d. Rayleigh fading model.

## V. PERFORMANCE ANALYSIS WITH USER CORRELATION

In Sections III and IV, we find that shared AoDs can result in high user correlation that does not vanish with large number of base-station antennas. We now characterize the impact of user channel correlation on the massive MIMO system performance.

The performance analysis requires special treatment of the channel model: For a spatial channel model, like (5), the distribution of the  $K$ -user channel  $\mathbf{H}$  is determined by the joint distribution of the gains and phases of *all*  $K$  users. However, the joint distribution of these spatial parameters is extremely hard to measure over-the-air. Additionally, it is well-known that the distribution of the parameters is highly dependent on the propagation environment [34].

In this section, we first review the Kronecker’s channel model, which captures both the base-station array and user correlation. Based on the statistical channel model, we characterize the effective SINR of massive MIMO with zero-forcing or conjugate beamforming. We then comment on the impact of user correlation by considering a special case that is motivated by channel measurements. The analysis in this section will be later examined based on measured channels in Section VI.

### A. Multiuser Channel With User Correlation

To capture the joint distribution of the  $K$  user downlink channel  $\mathbf{H} \in \mathbb{C}^{K \times M}$ , we adopt the Kronecker’s channel model. The downlink channel  $\mathbf{H}$  reads [40]

$$\mathbf{H} = (\mathbf{R}^u)^{1/2} \mathbf{Z} \left[ (\mathbf{R}^b)^{1/2} \right]^T, \quad (10)$$

where  $(\mathbf{R}^u)^{1/2}$  and  $(\mathbf{R}^b)^{1/2}$  are the Cholesky decomposition of the user covariance matrix  $\mathbf{R}^u \in \mathbb{R}^{K \times K}$  and the base-station array correlation matrix  $\mathbf{R}^b \in \mathbb{R}^{M \times M}$ , respectively. The channel correlation between User  $k_1$  and User  $k_2$  is then

the element on the  $k_1$ -th row and  $k_2$ -th column in  $\mathbf{R}^u$ . Thus, both  $\mathbf{R}^u$  and  $\mathbf{R}^b$  are symmetric matrices. And each entry of  $\mathbf{Z} \in \mathbb{C}^{K \times M}$  follows an i.i.d. standard complex Gaussian distribution. Note that (10) allows us to assign any user and base-station array correlation.

The model (10) generalizes many past used massive MIMO models. For example, massive MIMO with base-station array correlation and no user correlation [25], [26], [4], [28], [29] is the special case when  $\mathbf{R}^u = \mathbf{I}_K$ . And i.i.d. Rayleigh fading [6], [7], [5], [1], [2], [8], [23] is the case when  $\mathbf{R}^u = \mathbf{I}_K$  and  $\mathbf{R}^b = \mathbf{I}_M$ . In the context of COST 2100 models [12], [13], model (10) is expected to capture the base-station and user correlation among users from the same “visible region”, i.e., users with small spatial separation.

It is noted that some past work assumes that each base-station user pair can have a different base-station array correlation. Such case can be captured by letting  $\mathbf{R}^b = \mathbf{I}_M$  and changing each row of  $\mathbf{Z}$  to follow complex Gaussian of  $\mathcal{CN}(\mathbf{0}_M, \mathbf{R}_k^b)$ , where  $\mathbf{R}_k^b \in \mathbb{R}^{M \times M}$  can differ across users. Notice that  $\text{vec}(\mathbf{Z}) \sim \mathcal{CN}(\mathbf{0}_{KM \times KM}, \tilde{\mathbf{R}}^b)$ , where the  $\tilde{\mathbf{R}}^b$  is a diagonal block matrix with diagonal blocks being  $\mathbf{R}_k^b$ . Thus, the analysis based on model (10) can be extended, if the *joint* distribution of  $\mathbf{R}_k^b$  is known. We consider the modeling of the joint distribution of  $\mathbf{R}_k^b$  to be an important future research direction that is beyond the focus of this paper. In Section VI, we will use numerical experiments to evaluate the analytical results in real propagation environments.

1) *Channel Estimation Model:* In this work, we adopt the following channel estimation model [41], [3]

$$\mathbf{H} = \hat{\mathbf{H}} + \tilde{\mathbf{H}}, \quad (11)$$

where  $\tilde{\mathbf{H}}$  is the estimation error matrix whose elements follow independent complex normal distribution<sup>1</sup> with zero mean and variance of  $\sigma_\tau^2$ . The modeled estimation error is independent

<sup>1</sup> If the channel covariance matrix is available, it is possible to leverage such second-order channel statistics to improve the channel estimation quality. For example, [4, Chapter 3] considers that the  $\mathbf{R}^u = \mathbf{I}_K$  and  $\mathbf{R}^b$  is perfectly available at the base-station. Such an assumption works well in environments where the covariance matrix  $\mathbf{R}^b$  is stable for a long time. Recent massive MIMO measurements demonstrate that the second-order channel statistics can also vary quickly in mobile environments [15], [16], [17], [18]. Thus, our analysis serves as a worst-case analysis for mobile massive MIMO systems. We consider the problem of incorporating a partially available channel correlation matrix for channel estimation improvement as an important future research direction.



of the estimated channel,  $\hat{\mathbf{H}}$ . The channel estimation quality is captured by the scalar<sup>2</sup>  $\sigma_\tau$ . Note that (11) is not limited to a specific channel estimation method and includes many channel estimation methods [32], [3], [4]. For example, for a TDD system using per-antenna MMSE estimator based on orthogonal uplink pilot sequences [1], [2], [3],  $\sigma_\tau$  equals  $\sqrt{\frac{1}{1+p_u}}$ , where  $p_u$  is the effective SNR of the uplink pilot sequence. Denote  $\hat{\mathbf{h}}_k$ ,  $\tilde{\mathbf{h}}_k$ , and  $\mathbf{v}_k$  as the estimated channel, estimation error, and beamforming weights of User  $k$ , respectively. The received signal at User  $k$  then equals [3], [4]

$$\mathbf{y}_k = \sqrt{\gamma_k} \hat{\mathbf{h}}_k^H \mathbf{v}_k s_k + \sum_{j \neq k} \sqrt{\gamma_k} \tilde{\mathbf{h}}_k^H \mathbf{v}_j s_j + w_k - \sqrt{\gamma_k} \tilde{\mathbf{h}}_k^H \mathbf{V} \mathbf{s}, \quad (12)$$

where  $w_k$  is the additive noise, and  $s_k$  is the transmitted symbol. The first term denotes the desired signal. And the other three terms in (12) represents the interference from the beamforming algorithm, noise, and interference from imperfect channel knowledge, respectively.

### B. Beamforming Methods

Based on the estimated channel matrix, the base-station computes the downlink precoding weights for data precoding. In this paper, we consider Zero-Forcing (ZF) and ConJugate (CJ) beamforming algorithms. For ZF and CJ, The beamforming matrix  $\mathbf{V}$  reads as [3]

$$\mathbf{V} = \begin{cases} \sqrt{d^{\text{ZF}}} \hat{\mathbf{H}}^H \left( \hat{\mathbf{H}} \hat{\mathbf{H}}^H \right)^{-1}, & \text{ZF} \\ \sqrt{d^{\text{CJ}}} \hat{\mathbf{H}}^H, & \text{CJ} \end{cases}. \quad (13)$$

where  $d^{\text{ZF}}$  and  $d^{\text{CJ}}$  are the normalization scalars for transmission power control.

Following the large body of past work [3], [4], [32], we capture the massive MIMO performance by computing the effective SINR of each user. Similar to past work, we assume that each user only knows the ratio between actual channel gain and the total interference power. This assumption is widely-adopted due to the channel hardening [8] effect in massive MIMO. By treating interference as a worst-case Gaussian noise, an ergodic achievable information rate of User  $k$  is given by  $r_k = \log(1 + \text{SINR}_k)$ , where  $\text{SINR}_k$  is the effective SINR of User  $k$ . We now derive the effective SINR for massive MIMO with user and base-station array correlation.

### C. Effective SINR Computation

The effective SINR for both CJ and ZF are presented in this subsection.

**Theorem 2** (CJ SINR). *If CJ beamforming algorithm in (13) is used, the effective SINR of User  $k$  satisfies*

$$\text{SINR}_k = \frac{d^{\text{CJ}} (R_{kk}^u \text{tr} \mathbf{R}^b - M \sigma_\tau^2)^2}{d^{\text{CJ}} (e_{k1} + e_{k2} + e_{k3}) + \frac{1}{\gamma_k} + \sigma_\tau^2 P}, \quad (17)$$

<sup>2</sup> Note that the large-scale channel fading differences among users can be directly captured by assigning a different  $\sigma_\tau$  to each user. The rate analysis in this section should also be updated accordingly. As the large-scale channel fading is not the focus of this paper, we adopt a single  $\sigma_\tau$  for notational simplicity.

where  $d^{\text{CJ}} = \frac{KP}{(\text{tr} \mathbf{R}^b \text{tr} \mathbf{R}^u - MK \sigma_\tau^2)}$ ,  $R_{kj}^u$  is the element on  $k$ -th row and  $j$ -th column in  $\mathbf{R}^u$ , and  $e_{k1}, e_{k2}, e_{k3}$  is given by (14), (15), (16).

The proof is relegated to Appendix VIII-C. Similarly, we present the SINR for ZF.

**Theorem 3** (ZF SINR). *Assume that the rank of the estimated channel  $\hat{\mathbf{H}}$  is no smaller than  $K$ . If ZF beamforming algorithm in (13) is used, the effective SINR of User  $k$  satisfies*

$$\text{SINR}_k = d^{\text{ZF}} \frac{\gamma_k}{1 + \gamma_k \sigma_\tau^2 P} = \frac{P}{E \left[ \sum_{k=1}^K \frac{1}{\lambda_k} \right]} \frac{\gamma_k}{1 + \gamma_k \sigma_\tau^2 P}, \quad (18)$$

where  $\lambda_k$  is the eigenvalues of matrix  $\hat{\mathbf{H}} \hat{\mathbf{H}}^H$  and the distribution of  $\hat{\mathbf{H}} \in \mathbb{C}^{K \times M}$  is given by

$$\text{vec} \left( \hat{\mathbf{H}} \right) \sim \mathcal{CN} \left( \mathbf{0}_{KM}, \mathbf{R}^u \otimes \mathbf{R}^b - \sigma_\tau^2 \mathbf{I}_K \otimes \mathbf{I}_M \right). \quad (19)$$

The proof is detailed in Appendix VIII-D. Theorem 2 and Theorem 3 presents the effective SINR of CJ and ZF based massive MIMO systems with correlation at both the users and the base-station. Note that the effective SINR of massive MIMO with ZF contains fewer terms than the SINR of massive MIMO with CJ. The main reason is that ZF projects the signal of other users onto the null space of the estimated channel vector. However, the power normalization scalar of ZF,  $d^{\text{ZF}}$ , is more involved than that of CJ. The complexity mainly comes from the matrix inversion over the estimated channel, which contains both user correlation and base-station array correlation.

If there exists no user or base-station array correlation, elements of  $\hat{\mathbf{H}}$  follow simple independent Gaussian distribution and  $d^{\text{ZF}}$  can be immediately computed. Directly compute  $d^{\text{ZF}}$  is challenging with correlation. If there exists only base-station correlation and no user correlation, the estimated user channels  $\hat{\mathbf{h}}_k$  are independent. Past work [29], [30], [32] exploits such independence across users to approximate the  $d^{\text{ZF}}$  in the large array regime where  $M \rightarrow \infty$ . In our analysis, the estimated user channels are no longer independent. Therefore, such approximation techniques cannot be directly applied to systems with both user and base-station correlation. We later will derive  $d^{\text{ZF}}$  without approximation for a special case in Section V-D.

### D. Impact of User Correlation

In this subsection, we use the SINR characterized in Theorem 2 and Theorem 3 for insights into the interplay of imperfect channel estimation and user correlation on the effective SINR. Inspired by over-the-air channel measurements in Section IV, we consider a special case of the downlink channel (10) as follows.

- **Condition C1:** The base-station array correlation is  $\mathbf{R}^b = \mathbf{I}_M$ .
- **Condition C2:** The  $K$  users are distributed in  $N$  clusters. The intra-cluster user correlation is modeled by  $\alpha_n \in [0, 1)$ , where  $n$  is the cluster index. The inter-cluster user correlation is captured by a constant  $\beta \in [0, 1)$ . The number of users in Cluster  $n$  is denoted by  $s_n$  such that

$$e_{k1} = \text{tr} \left[ (\mathbf{R}^b)^T \mathbf{R}^b \right] (R_{kk}^u)^2 - 2\text{tr} \mathbf{R}^b \sigma_\tau^2 R_{kk}^u + M\sigma_\tau^4, \quad (14)$$

$$e_{k2} = \sum_{j=1, j \neq k}^K \left\{ \text{tr} \left[ (\mathbf{R}^b)^T \mathbf{R}^b \right] \left[ R_{kk}^u R_{jj}^u + (R_{kj}^u)^2 \right] + \left[ (\text{tr} \mathbf{R}^b)^2 - \sum_m (R_{mm}^b)^2 \right] (R_{kj}^u)^2 \right\}, \quad (15)$$

$$e_{k3} = \sum_{j=1, j \neq k}^K \left\{ -\sigma_\tau^2 \text{tr} \mathbf{R}^b (R_{kk}^u + R_{jj}^u) + M\sigma_\tau^4 \right\}, \quad (16)$$

$K = \sum_{n=1}^N s_n$ . Thus, the diagonals of  $\mathbf{R}^u$  are 1. And the off-diagonal elements  $\mathbf{R}_{kj}^u$  equals  $\alpha_n$  if both User  $k$  and User  $j$  are in Cluster  $n$ , or equals  $\beta$  when User  $k$  and User  $j$  are from different clusters.

We note that C1 might not hold in practical massive MIMO systems due to the small spacing of base-station antennas. Thus, Section V-D should be treated as a special case study for understanding the impact of user correlation. For general massive MIMO systems with base-station correlation, Theorem 2, 3 should be adopted.

**Corollary 2.** *Under condition C1, if CJ beamforming algorithm in (13) is used, the effective SINR of User  $k$  satisfies that*

$$\text{SINR}_k = \frac{M \frac{P}{K} (1 - \sigma_\tau^2)}{1 + \gamma_k P + M \frac{\gamma_k P}{K(1 - \sigma_\tau^2)} \sum_{j \neq k} (R_{kj}^u)^2}, \quad (20)$$

where  $R_{kj}^u$  is the element on  $k$ -th row and  $j$ -th column in  $\mathbf{R}^u$ .

The proof is immediate by substituting C1 into Theorem 2 and algebraic manipulations. Corollary 2 captures the effect of channel estimation error and user correlation on effective SINR. The three terms on the denominator capture the receiver noise, interference from limited number of base-station antennas, and interference from user correlation. The imperfect channel estimation reduces the SINR by lowering the signal power and increasing the inter-user correlation. The interference power from limited number of base-station antennas does not increase with  $M$ , which is similar to previous results [3], [4] for systems without user correlation. More importantly, the user correlation leads to a new interference whose power scales *linearly* with the number of base-station antennas. Therefore, the new interference from user correlation limits the performance of massive MIMO systems with CJ. We now derive the effective SINR for ZF.

**Corollary 3.** *Under condition C1 and C2, if ZF beamforming algorithm in (13) is used, the effective SINR satisfies that*

$$\text{SINR}_k = \frac{d^{\text{ZF}} \gamma_k}{1 + \gamma_k \sigma_\tau^2 P}, \quad (21)$$

where the power normalization scalar  $d^{\text{ZF}}$ , which is given by (22).

The proof can be found in Appendix VIII-E. The first step is to show that, under C1,  $\mathbf{H}\mathbf{H}^H$  is a complex Wishart matrix with scale matrix of  $\mathbf{R}^u - \sigma_\tau^2 \mathbf{I}_K$ . The rest of proof is matrix manipulations on the matrix inversion trace via the Sherman—Morrison—Woodbury matrix identity under C2.

Interestingly, under the described correlation structure C1 and C2, the effective SINR can be derived in closed-form. The SINR loss from user correlation is captured by a complex constant in (22). And the SINR loss constant is independent of the number of base-station antennas  $M$ . Therefore, ZF with user correlation achieve the same SINR as ZF without user correlation but with a reduced large scale channel gain. And the SINR loss factor  $d^{\text{ZF}}$  (22) is monotonically decreasing on  $\alpha_n$ , which matches the intuition that user correlation reduces effective SINR.

A crucial performance metric of any spatial multiplexing system is the number of users that can be multiplexed. For massive MIMO systems with i.i.d. Rayleigh fading channel, the user channels become more orthogonal as  $M$  increases. As a result, when  $M$  increases, a growing number of users (proportional to  $M$ ) can be supported while maintaining the same effective SINR [3].

When shared AoDs happen, the mean of the square of the user correlation converges to a positive constant as  $M$  grows. For a group of correlated users, it might be natural to expect that such user correlation limits the multiplexing gain. However, the analysis shows differently. Consider a special case when there are  $K$  users with user correlations being  $\alpha$ . The power normalization scalar  $d^{\text{ZF}}$  in (22) then becomes

$$d^{\text{ZF}} = \frac{M - K}{K} (1 - \sigma_\tau^2 - \alpha) \left[ 1 + \frac{\alpha}{1 - \sigma_\tau^2 + \alpha (K - 2)} \right] P. \quad (23)$$

The SINR loss from spatial multiplexing more correlated users converges to a fixed point of  $(1 - \sigma_\tau^2 - \alpha)$  as  $K$  increases. Therefore, with ZF, the number of users  $K$  can still scale linearly with  $M$  while the per-user SINR stays the same. The main reason that the user correlation does not reduce the level of multiplexing is that the dimensions of the null space of the beamformer  $(M - K)$  also grows linearly with  $M$ . In Section VI, we use numerical experiments to examine the effective SINR analysis.

Finally, we remark that our analysis focuses on single-cell systems and does not capture the pilot contamination effect [4], [3] from pilot reuse of neighboring cells. Similar to the case of no user correlation, decontamination techniques should be applied to overcome the coherence interference from the pilot reuse in systems with user correlation. For example, [30] recently demonstrates that multicell joint ZF or MMSE transmission can reject the coherent interference from pilot contamination if the pilot-sharing users' base-station array covariance matrix is asymptotically linearly independent, which is most likely to hold over-the-air.

$$d^{\text{ZF}} = \left\{ \sum_{n=1}^N \frac{s_n [f_n - (\alpha_n - \beta)]}{f_n (1 - \sigma_\tau^2 - \alpha_n)} - \frac{\beta \sum_{n=1}^N s_n / f_n^2}{1 + \beta \sum_{n=1}^N s_n / f_n} \right\}^{-1}, \text{ where } f_n = 1 - \sigma_\tau^2 - s_n \beta + \alpha_n (s_n - 1). \quad (22)$$

## VI. NUMERICAL EVALUATIONS

Section V presents the effective SINR of massive MIMO with user and base-station array correlation. We first evaluate the accuracy of the theoretical analysis over channel model generated with the statistical channel model (10). The measured channels [21] are then used to validate the theoretical analysis. During the evaluation, we consider base-station with different number of antennas and evaluate the downlink user rate. Finally, the power channel estimation error in (11) is  $\sigma_\tau^2 = 0.01$ .

We first consider the performance of CJ and ZF over channel in (10). The base-station beamforms to 6 users from two clusters, each with 3 users. Users are assumed to be of similar large-scale fading. And the transmission power  $P$  is scaled so that the interference-free SNR of each user, i.e.,  $PM\gamma_k/K$ , is 20 dB. Hence, the product of the transmission power  $P$ , and the large scale channel gain equals  $100K/M$ . The base-station array correlation matrix is  $\mathbf{I}_M$ . The inter-cluster correlation level  $\beta$  is assumed to be 0.1. For Cluster 2, the intra-cluster correlation is 0.5. We experiment different level of intra-cluster correlation for Cluster 1.

Fig. 7 presents the achievable rates of Cluster 1 users under both CJ and ZF. The numerical experiments match the theoretical analysis in Section V. As expected, the achievable rate reduces as the user correlation level reduces. The simulations also confirm that CJ leads to a much lower rate compared to ZF when user correlation exists.

We now comment on the impact of user correlation on spatial multiplexing gain. Consider an  $M$ -antenna base-station adopts ZF to beamform to  $K$  users with similar large scale channel gain. And the total transmission power times large scale channel gain equals 100. We assume that the number of base-station antenna  $M$  and user number  $K$  both increase at different fixed ratios. We first consider simulated channel model (10) with user correlations of 0.5 and no base-station correlation. Fig. 8 presents the total downlink achievable rate as a function of  $M$ . As the number of base-station antennas increases, the sum achievable rate can increase linearly with the number of base-station antenna. Hence, we confirm the analysis on that even with user correlation, the degree of multiplexing can still scale linearly with  $M$ .

Finally, we use measured channels to demonstrate that the degree of multiplexing of correlated users can also grow linearly with  $M$  in real-world propagation. We adopt all users from each measured NLOS cluster. The user channels hence are mutually correlated. We examine all five NLOS clusters individually by using the measurements on the 52-th subcarrier. For each NLOS cluster, the number of users  $K$  increases with  $M$  and different fixed ratios. Fig. 8 present the sum rate based on the measured channel and the analytical derivation. The statistical channel model (10) based analysis matches well with simulations based on measured channel. By serving a

growing number of correlated users, a linearly achievable rate growth can be achieved with ZF. Hence, we conclude that user correlation itself does not limit the spatial multiplexing gain of massive MIMO. With proper beamforming, like ZF, a massive MIMO base-station can overcome user correlation and spatial multiplex users of size proportional to its number of antennas.

## VII. CONCLUSION

In this work, we accept the fact that user correlation can happen in massive MIMO due to shared AoDs. Our analysis proves that, with shared AoDs, the mean of the square of the user correlation converges to a positive fixed point in the large array regime. We measure and open-accessed a new massive MIMO channel data set. We use measured channels to examine the user correlation in a real-world propagation environment. The measurements show that adding more antennas barely reduces the user correlation between close-by users when the number of base-station antennas  $M > 36$ . And more than 28.6% of far-away user pairs have correlation higher than twice of that in i.i.d. Rayleigh fading model. Via spatial signal processing, we confirm that shared AoDs are the root cause of the measured high user correlation. To understand the impact of user correlation, we analyze the effective SINR of systems with user and base-station array correlation. Due to the user correlation, conjugate beamforming systems suffer an inter-user interference that scales linearly with the number of base-station antennas. However, with more base-station antennas, zero-forcing beamforming systems can still support a linearly growing number of users while maintaining the same level of SINR. We further validate the analysis by numerical experiments based on simulated and measured channels. The presented results collectively demonstrate that a proper massive MIMO design could effectively mitigate the user correlation and make spatial multiplexing correlated users attractive.

## VIII. APPENDICES

### A. Proof of Theorem 1

We prove by computing the denominator and the numerator of (2). Denote  $(\theta_x^l, \theta_y^l)$  as  $\theta^l$ . By the array response vector definition in (6),  $\frac{1}{M} \mathbf{a}(\theta)^H \mathbf{a}(\theta) = 1$ . We first compute  $|\mathbf{h}_1|$  as

$$\begin{aligned} \frac{1}{M} |\mathbf{h}_1|^2 &= \sum_{l=1}^L g_1^l \\ &+ \frac{1}{M} \sum_{l_1=1}^L \sum_{l_2 \neq l_1}^L \sqrt{g_1^{l_1} g_1^{l_2}} e^{j(\phi_1^{l_1} - \phi_1^{l_2})} \mathbf{a}^H(\theta^{l_1}) \mathbf{a}(\theta^{l_2}), \end{aligned} \quad (24)$$

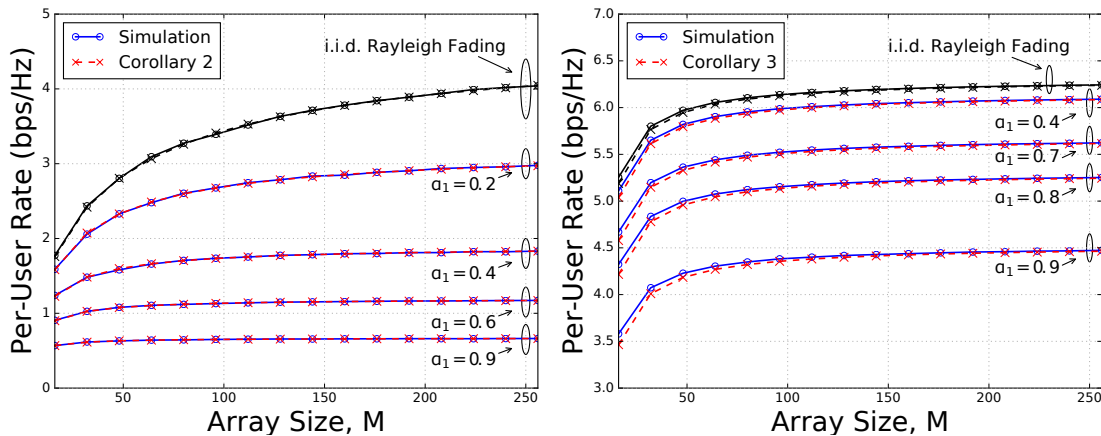


Fig. 7. Achievable rates of massive MIMO with user correlation and imperfect channel knowledge. Massive MIMO systems in figure left and right adopt conjugate and zero-forcing beamforming algorithm, respectively. The total transmission power constraint  $P$  is inversely proportional to the number of base-station antennas  $M$ .

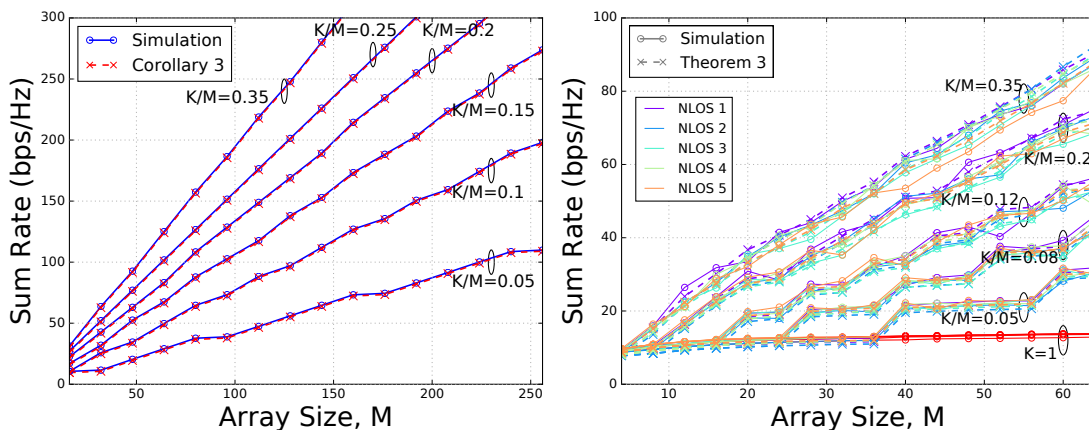


Fig. 8. Zero-forcing massive MIMO performance with user correlation. With ZF, the number of served users  $K$  can still scale linearly with the number of base-station antennas  $M$ . The left is based on simulated channels, while the right is based on measured channel. As a result, for massive MIMO with user correlation, the sum rate increases linearly with  $M$ . The total transmission power constraint  $P$  is fixed and does not change with  $M$ . The number of users  $K$  is selected as  $\max\{1, \lfloor M(K/M) \rfloor\}$ , where  $\lfloor \cdot \rfloor$  is the floor operator.

which is immediate via algebraic manipulations. Similarly, we compute the numerator of (2) as

$$\begin{aligned} \frac{1}{M} \mathbf{h}_1^H \mathbf{h}_2 &= \sum_{l=1}^L \sqrt{g_1^l g_2^l} e^{j(\phi_2^l - \phi_1^l)} \\ &+ \frac{1}{M} \sum_{l_1=1}^L \sum_{l_2 \neq l_1}^L \sqrt{g_1^{l_1} g_2^{l_2}} e^{j(\phi_1^{l_1} - \phi_2^{l_2})} \mathbf{a}^H(\boldsymbol{\theta}^{l_1}) \mathbf{a}(\boldsymbol{\theta}^{l_2}) \end{aligned} \quad (25)$$

By Lemma 1 in Appendix VIII-F, for two independent uniform random angles  $\boldsymbol{\theta}^{l_1}$  and  $\boldsymbol{\theta}^{l_2}$ ,  $\frac{1}{M} \mathbf{a}^H(\boldsymbol{\theta}^{l_1}) \mathbf{a}(\boldsymbol{\theta}^{l_2}) \xrightarrow{P} 0$  as  $M \rightarrow \infty$ . Note that  $\phi_2^l - \phi_1^l$  follows uniform distribution on  $[0, 4\pi]$ . The continuous mapping theorem completes the proof by substituting (24), (25) into (2).

### B. Proof of Corollary 1

Based on Theorem 1, we now characterize  $c(\mathbf{h}_1, \mathbf{h}_2)$ . Let  $\tilde{c}$  denote  $\left| \sum_{l=1}^L \sqrt{\frac{g_1^l}{\sum_{l=1}^L g_1^l} \frac{g_2^l}{\sum_{l=1}^L g_2^l}} e^{j\tilde{\phi}^l} \right|$ . We start with the mean computation. After some manipulations,  $E[\tilde{c}^2]$  equals (26). Using that  $\tilde{\phi}^{l_1}$  follows independent uniform distribution on

$[0, 2\pi]$  completes the proof of (8). Since  $\text{Var}[\tilde{c}^2] = E[\tilde{c}^4] - E^2[\tilde{c}^2]$ , we now finish the proof by using (26) and computing  $E[\tilde{c}^4]$  as

$$E[\tilde{c}^4] = \left( \frac{\sum_{l=1}^L g_1^l g_2^l}{\sum_{l=1}^L g_1^l \sum_{l=1}^L g_2^l} \right)^2 + \frac{\sum_{l_1=1}^L \sum_{l_2=1, l_2 \neq l_1}^L g_1^{l_1} g_2^{l_1} g_1^{l_2} g_2^{l_2}}{\left( \sum_{l=1}^L g_1^l \sum_{l=1}^L g_2^l \right)^2}. \quad (27)$$

### C. Effective SINR of Conjugate Beamforming

Based on the conjugate beamforming weights (13), we rewrite the signal model in (12) as

$$\begin{aligned} \mathbf{y}_k &= \sqrt{d^{CJ} \gamma_k} E[\hat{\mathbf{h}}_k^H \hat{\mathbf{h}}_k] s_k \\ &+ \sqrt{d^{CJ} \gamma_k} \left( \hat{\mathbf{h}}_k^H \hat{\mathbf{h}}_k - E[\hat{\mathbf{h}}_k^H \hat{\mathbf{h}}_k] \right) s_k \\ &+ \sqrt{d^{CJ} \gamma_k} \sum_{j \neq k} \hat{\mathbf{h}}_k^H \hat{\mathbf{h}}_j s_j + w_k - \sqrt{\gamma_k} \tilde{\mathbf{h}}_k^H \mathbf{V} s. \end{aligned}$$

The first term is the signal, and the other four terms are interference and noise. The noise power  $\text{Var}[w_k]$  equals 1. We now derive the power of the signal and interference terms.

Equation (41) in Lemma 2 gives the covariance matrix of  $\hat{\mathbf{h}}_k^H \hat{\mathbf{h}}_k$ . The signal power equals

$$\text{Var} \left[ \sqrt{d_k} \gamma_k E \left[ \hat{\mathbf{h}}_k^H \hat{\mathbf{h}}_k \right] s_k \right]^2 = d_k \gamma_k (R_{kk}^u \text{tr} \mathbf{R}_b - M \sigma_\tau^2)^2. \quad (28)$$

By (42) in Lemma 2,  $\hat{\mathbf{h}}_k \sim \mathcal{CN}(\mathbf{0}, R_{kk}^u \mathbf{R}^b - \sigma_\tau^2 \mathbf{I}_M)$ . Applying Lemma 3, the beamforming uncertainty interference power can be derived as (29). By (41) in Lemma 2, we have that the interference from channel non-orthogonality power is

$$\begin{aligned} & \text{Var} \left( \sqrt{d^{\text{CJ}}} \gamma_k \sum_{j \neq k} \hat{\mathbf{h}}_k^H \hat{\mathbf{h}}_j s_j \right) \\ &= d^{\text{CJ}} \gamma_k \sum_{j \neq k} E \left( \left| \hat{\mathbf{h}}_k^H \hat{\mathbf{h}}_j \right|^2 \right) \\ &= d^{\text{CJ}} \gamma_k \sum_{j \neq k} \sum_m \sum_{m'} \hat{h}_{km}^H \hat{h}_{km}' \hat{h}_{jm}^H \hat{h}_{jm}' \\ &= d^{\text{CJ}} \gamma_k (e_{k2} + e_{k3}). \end{aligned} \quad (30)$$

The last step is based on Lemma 2 and Isserlis' theorem [42]. The algebraic manipulations are omitted due to the space constraint. The interference power from the imperfect channel equals

$$\begin{aligned} \text{Var} \left[ \sqrt{\gamma_k} \tilde{\mathbf{h}}_k^H \mathbf{V} \mathbf{s} \right] &= \gamma_k \sigma_\tau^2 \text{tr} E \left[ \mathbf{V} \mathbf{s} \mathbf{s}^H \mathbf{V}^H \right] \\ &= \gamma_k \sigma_\tau^2 \text{tr} E \left[ \mathbf{s} \mathbf{s}^H \right] \text{tr} E \left[ \mathbf{V} \mathbf{V}^H \right] = \gamma_k \sigma_\tau^2 P. \end{aligned} \quad (31)$$

Combining (28), (29), (30), (31) leads to the SINR expression in Theorem 2. Finally, by using (42) in Lemma 2, we complete the proof by computing the normalization scalar as

$$d^{\text{CJ}} = \frac{P}{\text{tr} E \left[ \hat{\mathbf{H}} \hat{\mathbf{H}}^H \right]} = \frac{P}{(\text{tr} \mathbf{R}^b \text{tr} \mathbf{R}^u - M K \sigma_\tau^2)}.$$

#### D. Effective SINR of Zero-forcing Beamforming

By plugging the ZF beamforming matrix in (13) into the signal model (12), the interference from the transmitted signal on the estimated channel is zero. Therefore, it suffices to compute the power of the signal and imperfect channel interference. The signal power satisfies that

$$\text{Var} \left[ \sqrt{\gamma_k} \hat{\mathbf{h}}_k^H \mathbf{v}_k s_k \right] = \text{Var} \left[ \sqrt{\gamma_k} \sqrt{d^{\text{ZF}}} s_k \right] = d^{\text{ZF}} \gamma_k.$$

By orthogonality principle,  $\hat{\mathbf{H}}$  is independent of the estimated channel and thus the computed beamforming matrix. The interference power from imperfect channel estimation is then

$$\begin{aligned} \text{Var} \left[ \sqrt{\gamma_k} \tilde{\mathbf{h}}_k^H \mathbf{V} \mathbf{s} \right] &= \gamma_k \sigma_\tau^2 \text{tr} E \left[ \mathbf{V} \mathbf{s} \mathbf{s}^H \mathbf{V}^H \right] \\ &= \gamma_k \sigma_\tau^2 \text{tr} E \left[ \mathbf{s} \mathbf{s}^H \right] \text{tr} E \left[ \mathbf{V} \mathbf{V}^H \right] = \gamma_k \sigma_\tau^2 P. \end{aligned} \quad (32)$$

Finally, we compute the power normalization scalar  $d^{\text{ZF}}$  as

$$d^{\text{ZF}} = \frac{P}{E \text{tr} \left[ \hat{\mathbf{V}} \hat{\mathbf{V}}^H \right]} = P \left\{ E \left[ \text{tr} \left( \hat{\mathbf{H}} \hat{\mathbf{H}}^H \right)^{-1} \right] \right\}^{-1}.$$

Notice that  $\hat{\mathbf{H}} \hat{\mathbf{H}}^H$  is a Hermitian matrix. The eigendecomposition gives that  $\mathbf{Q} \Lambda \mathbf{Q}^H$ , where  $\Lambda$  is the diagonal eigenvalue matrix. We thus have that

$$\begin{aligned} \text{tr} \left( \hat{\mathbf{H}} \hat{\mathbf{H}}^H \right)^{-1} &= \text{tr} \left( \mathbf{Q} \Lambda \mathbf{Q}^H \right)^{-1} = \text{tr} \left( \mathbf{Q} \Lambda^{-1} \mathbf{Q}^H \right) \\ &= \text{tr} \left( \Lambda \mathbf{Q} \mathbf{Q}^H \right)^{-1} = \text{tr} \left( \Lambda^{-1} \right). \end{aligned}$$

The proof is then complete by the captured distribution of  $\hat{\mathbf{H}}$  as in (43).

#### E. Proof of Corollary 3

Based on Theorem 3, it is sufficient to compute the  $d^{\text{ZF}}$ . The distribution of  $\hat{\mathbf{H}}$  is given in (19). Under C1,  $\mathbf{R}^b = \mathbf{I}_M$ . The estimated channel follows matrix Gaussian distribution as  $\hat{\mathbf{H}} \sim \mathcal{MN}(\mathbf{0}, \mathbf{R}^u - \sigma_\tau^2 \mathbf{I}_K, \mathbf{I}_M)$ . Therefore, each column of  $\hat{\mathbf{H}}$  follows  $\mathcal{CN}(\mathbf{0}_M, \mathbf{R}^u - \sigma_\tau^2 \mathbf{I}_K)$ . Hence,  $\hat{\mathbf{H}} \hat{\mathbf{H}}^H$  is a complex Wishart matrix with  $M$  degree of freedom and scale matrix of  $\mathbf{R}^u - \sigma_\tau^2 \mathbf{I}_K$ . We now derive the matrix inversion trace as

$$\begin{aligned} E \left[ \text{tr} \left( \hat{\mathbf{H}} \hat{\mathbf{H}}^H \right)^{-1} \right] &= \text{tr} E \left[ \left( \hat{\mathbf{H}} \hat{\mathbf{H}}^H \right)^{-1} \right] \\ &= \frac{\text{tr} \left( \mathbf{R}^u - \sigma_\tau^2 \mathbf{I}_K \right)^{-1}}{M - K}. \end{aligned} \quad (33)$$

Here, the last step is by the Wishart matrix inverse theorem, which is detailed in Lemma 6. The power normalization factor  $d^{\text{ZF}}$  (13) then reads

$$d^{\text{ZF}} = \frac{P(M - K)}{\text{tr} \left( \mathbf{R}^u - \sigma_\tau^2 \mathbf{I}_K \right)^{-1}}. \quad (34)$$

It then suffices to compute  $\text{tr} \left( \mathbf{R}^u - \sigma_\tau^2 \mathbf{I}_K \right)^{-1}$ . Define  $\tilde{\mathbf{R}}^u = \mathbf{R}^u - \sigma_\tau^2 \mathbf{I}_K - \beta \mathbf{1}_K \mathbf{1}_K^T$ . We now compute the trace of  $\left( \mathbf{R}^u - \sigma_\tau^2 \mathbf{I}_K \right)^{-1} = \left( \tilde{\mathbf{R}}^u + \beta \mathbf{1}_K \mathbf{1}_K^T \right)^{-1}$  as follows. We first decompose the matrix inverse via Lemma 5, the Sherman—Morrison—Woodbury matrix identity.

Notice that  $\tilde{\mathbf{R}}^u$  can be re-written as a block matrix with all zeros off-diagonal blocks and diagonal blocks being  $\tilde{\mathbf{R}}_n^u$ . Each diagonal block  $\tilde{\mathbf{R}}_n^u$  have diagonal values of  $\delta = 1 - \sigma_\tau^2 - \beta$  and off-diagonal values of  $c_n = \alpha_n - \beta$ . To derive  $\left( \tilde{\mathbf{R}}^u \right)^{-1}$ , it then suffices to compute  $\left( \tilde{\mathbf{R}}_n^u \right)^{-1}$ , which is given by Lemma 4 as

$$\begin{aligned} \left( \tilde{\mathbf{R}}_n^u \right)^{-1} &= \frac{\delta + (s - 1) c_n}{[\delta + (s - 1) c_n] (\delta - c_n)} \mathbf{I}_K - \\ & \quad \frac{c_n}{[\delta + (s - 1) c_n] (\delta - c_n)} \mathbf{1}_{s_n \times s_n}. \end{aligned} \quad (36)$$

---


$$E \left[ \tilde{c}^2 \right] = \frac{1}{\sum_{l_1} g_1^{l_1} \sum_{l_2} g_2^{l_2}} \left\{ \sum_{l_1=1}^L g_1^{l_1} g_2^{l_1} + \sum_{l_1=1}^L \sum_{l_2=1, l_2 \neq l_1}^L \sqrt{g_1^{l_1} g_2^{l_1} g_1^{l_2} g_2^{l_2}} E \left[ e^{-j(\tilde{\phi}^{l_1} - \tilde{\phi}^{l_2})} \right] \right\}. \quad (26)$$



$$\text{Var} \left[ \sqrt{\gamma_k} d \left( \hat{\mathbf{h}}_k^H \hat{\mathbf{h}}_k - E \left[ \hat{\mathbf{h}}_k^H \hat{\mathbf{h}}_k \right] \right) s_k \right] = \gamma_k d^{\text{CJ}} \left\{ \text{tr} \left[ (\mathbf{R}^b)^T \mathbf{R}^b \right] (R_{kk}^u)^2 - 2 \text{tr} \mathbf{R}^b \sigma_\tau^2 R_{kk}^u + M \sigma_\tau^4 \right\}. \quad (29)$$

$$\left( \tilde{\mathbf{R}}^u + \beta \mathbf{1}_K \mathbf{1}_K^T \right)^{-1} = \left( \tilde{\mathbf{R}}^u \right)^{-1} - \beta \left( \tilde{\mathbf{R}}^u \right)^{-1} \mathbf{1}_{K \times K} \left( \tilde{\mathbf{R}}^u \right)^{-1} \left( \mathbf{1} + \beta \mathbf{1}_K^T \left( \tilde{\mathbf{R}}^u \right)^{-1} \mathbf{1}_K \right)^{-1}. \quad (35)$$

We now compute the second term on the right of (35). We first compute the constant scalar as

$$\begin{aligned} & 1 + \beta \mathbf{1}_K^T \left( \tilde{\mathbf{R}}^u \right)^{-1} \mathbf{1}_K \\ &= 1 + \sum_{n=1}^N \frac{s_n}{[1 - \sigma_\tau^2 - \beta + (s_n - 1)(\alpha_n - \beta)]}. \end{aligned} \quad (37)$$

After some linear algebraic manipulations, the trace of the matrix products equals

$$\begin{aligned} & \text{tr} \left( \left( \tilde{\mathbf{R}}^u \right)^{-1} \mathbf{1}_{K \times K} \left( \tilde{\mathbf{R}}^u \right)^{-1} \right) \\ &= \sum_{n=1}^N \frac{s_n}{[\delta + (s_n - 1)c_n]^2}, \end{aligned} \quad (38)$$

where the last step is immediate by matrix manipulations with the block matrix  $\left( \tilde{\mathbf{R}}^u \right)^{-1}$  derived in (36). We now expand the trace of (35) as in (39). By plugging (36), (37), (38) into above, we can compute the  $\text{tr} \left( \mathbf{R}^u - \sigma_\tau^2 \mathbf{I}_K \right)^{-1}$  with algebraic manipulations. The proof is then complete with (34).

## F. Useful Lemmas

**Lemma 1.** *In the large array regime, the normalized dot product of two array response vectors (6) with uniform random angles converges in probability to 0, i.e.,*

$$\frac{1}{M} \mathbf{a}^H(\boldsymbol{\theta}_1) \mathbf{a}(\boldsymbol{\theta}_2) \xrightarrow{p} 0, \text{ as } M \rightarrow \infty. \quad (40)$$

*Proof.* Note that Proposition 2 in [10] provides the mean and variance of  $\frac{1}{M} \mathbf{a}^H(\boldsymbol{\theta}_1) \mathbf{a}(\boldsymbol{\theta}_2)$ . The proof is then immediate by substituting the mean and variance into the Chebyshev's Inequality.  $\square$

**Lemma 2.** *Under model (10) and (11), the estimated channel  $\hat{\mathbf{H}}$  satisfies that*

$$E \left[ \hat{\mathbf{h}}_k \hat{\mathbf{h}}_j^H \right] \begin{cases} R_{kk}^u \mathbf{R}^b - \sigma_\tau^2 \mathbf{I}_M, & \text{if } k = j \\ R_{kj}^u \mathbf{R}^b, & \text{if } k \neq j \end{cases}. \quad (41)$$

where  $R_{kj}^u$  is the element of  $\mathbf{R}^u$  on the  $k$ -th row and  $j$ -th column. And  $\hat{\mathbf{H}}$  also satisfies that

$$E \left[ \hat{\mathbf{H}} \hat{\mathbf{H}}^H \right] = (\text{tr} \mathbf{R}^b) \mathbf{R}^u - M \sigma_\tau^2 \mathbf{I}_K. \quad (42)$$

*Proof.* By (10) and (11), both the perfect channel and estimation error both follow matrix normal distribution as  $\mathbf{H} \sim \mathcal{MN}(\mathbf{0}, \mathbf{R}_u, \mathbf{R}_b)$  and  $\tilde{\mathbf{H}} \sim (\mathbf{0}, \sigma_\tau^2 \mathbf{I}_K, \mathbf{I}_M)$ . By orthogonality

principle, the estimated channel is independent of the channel and we have

$$\text{vec} \left( \hat{\mathbf{H}} \right) \sim \mathcal{CN}(\mathbf{0}, \mathbf{R}_u \otimes \mathbf{R}_b - \sigma_\tau^2 \mathbf{I}_K \otimes \mathbf{I}_M). \quad (43)$$

Here, this step is immediate by the fact that a linear transformed Gaussian vector is still Gaussian. Matrix manipulations on the Kronecker product completes the proof of (41). Finally, using (41) and the fact that  $E \left[ \hat{\mathbf{h}}_k^H \hat{\mathbf{h}}_j \right] = \text{tr} E \left[ \hat{\mathbf{h}}_k \hat{\mathbf{h}}_j^H \right]$ , (42) is immediate with matrix manipulations.  $\square$

**Lemma 3.** *For  $M$ -element complex Gaussian vector  $\mathbf{x}$  that follows  $\mathcal{CN}(\mathbf{0}, \mathbf{R})$ , it follows that*

$$\text{Var} [\mathbf{x}^H \mathbf{x}] = \text{tr} (\mathbf{R}^T \mathbf{R}). \quad (44)$$

*Proof.* The variance is directly available via expanding  $\text{Var} [\mathbf{x}^H \mathbf{x}]$  as  $E \left[ \left( \sum_{m=1}^M x_m^2 \right)^2 \right] - \left[ \sum_{m=1}^M E(x_m^2) \right]^2$ . The proof is then immediate by leveraging the fact that  $E[x_m^4] = 2R_{kk}^2$  and  $E[x_m^2 x_{m'}^2] = R_{mm} R_{m'm'} + R_{mm'}^2$ , for  $m \neq m'$ . The algebraic manipulations are omitted due to space constraint, and details are available in [42].  $\square$

**Lemma 4.** *For a  $s \times s$  real matrix with diagonals being  $\delta$  and off-diagonals being  $c$ , the inverse is a matrix with the diagonal elements being  $\frac{\delta + (s-2)c}{[\delta + (s-1)c](\delta - c)}$  and the off-diagonal elements being  $-\frac{c}{[\delta + (s-1)c](\delta - c)}$ .*

*Proof.* We compute  $\mathbf{R}_n^{-1}$  by splitting  $\mathbf{R}_n$  as  $\mathbf{R}_n = (\delta - \alpha) \mathbf{I}_{s_n} + \alpha \mathbf{1}_{s_n \times s_n}$ . To compute the inverse of  $\mathbf{R}_n$ , we utilize the Sherman—Morrison—Woodbury matrix identity, which is detailed by Lemma 5. The proof is complete by some algebraic manipulations.  $\square$

**Lemma 5.** [43, Section 2.1.3] *Let matrix  $\mathbf{A} \in \mathbb{C}^{n \times n}$  and  $\mathbf{U}, \mathbf{V} \in \mathbb{C}^{n \times k}$ . If  $\mathbf{A}$  and  $(\mathbf{I} + \mathbf{V}^H \mathbf{A}^{-1} \mathbf{U})$  are invertible, then it holds that  $(\mathbf{A} + \mathbf{U} \mathbf{V})^{-1} = \mathbf{A}^{-1} - \mathbf{A}^{-1} \mathbf{U} (\mathbf{I} + \mathbf{V} \mathbf{A}^{-1} \mathbf{U})^{-1} \mathbf{V} \mathbf{A}^{-1}$ .*

**Lemma 6** (Wishart Matrix Inversion). [44, Theorem 4] *Let  $\mathbf{A} \in \mathbb{C}^{K \times K}$  follow complex Wishart matrix distribution with scale matrix of  $\mathbf{R} \in \mathbb{R}^{K \times K}$  and  $M$  degrees of freedom. If  $M > K$ , then*

$$E(\mathbf{A}^{-1}) = \frac{\mathbf{R}^{-1}}{M - K}. \quad (45)$$

## AVAILABILITY OF DATA AND MATERIALS

The measured massive channels are open-accessed, and available for free download at [21].

$$\text{tr}(\mathbf{R}^u - \sigma_\tau^2 \mathbf{I}_K)^{-1} = \text{tr}(\tilde{\mathbf{R}}^u)^{-1} - \beta \text{tr} \left[ \left( \tilde{\mathbf{R}}^u \right)^{-1} \mathbf{1}_{K \times K} \left( \tilde{\mathbf{R}}^u \right)^{-1} \right] \left( 1 + \beta \mathbf{1}_K^T \left( \tilde{\mathbf{R}}^u \right)^{-1} \mathbf{1}_K \right)^{-1}. \quad (39)$$

## ACKNOWLEDGEMENT

We want to thank Mr. Xing Zhang for his help during the channel data measurement. We also want to thank Dr. Clayton Shepard for building and supporting the Argos massive MIMO platform [37].

## REFERENCES

- [1] H. Q. Ngo, E. G. Larsson, and T. L. Marzetta, "Energy and spectral efficiency of very large multiuser MIMO systems," vol. 61, no. 4, pp. 1436–1449, 2013.
- [2] H. Yang and T. L. Marzetta, "Performance of conjugate and zero-forcing beamforming in large-scale antenna systems," vol. 31, no. 2, pp. 172–179, 2013.
- [3] T. Marzetta, E. G. Larsson, H. Yang, and H. Ngo, *Fundamentals of massive MIMO*, Cambridge University Press, Cambridge, United Kingdom, 2016.
- [4] E. Björnson, J. Hoydis, and L. Sanguinetti, "Massive MIMO networks: Spectral, energy, and hardware efficiency," *Foundations and Trends® in Signal Processing*, vol. 11, no. 3-4, pp. 154–655, 2017.
- [5] E. G. Larsson, O. Edfors, F. Tufvesson, and T. L. Marzetta, "Massive MIMO for next generation wireless systems," vol. 52, no. 2, pp. 186–195, 2014.
- [6] T. L. Marzetta, "Noncooperative cellular wireless with unlimited numbers of base station antennas," vol. 9, no. 11, pp. 3590–3600, November 2010.
- [7] F. Rusek, D. Persson, B. K. Lau, E. G. Larsson, T. L. Marzetta, O. Edfors, and F. Tufvesson, "Scaling Up MIMO: Opportunities and Challenges with Very Large Arrays," vol. 30, no. 1, pp. 40–60, Jan 2013.
- [8] B. M. Hochwald, T. L. Marzetta, and V. Tarokh, "Multiple-antenna channel hardening and its implications for rate feedback and scheduling," vol. 50, no. 9, pp. 1893–1909, Sept 2004.
- [9] H. Q. Ngo, E. G. Larsson, and T. L. Marzetta, "Aspects of favorable propagation in massive MIMO," in *2014 22nd European Signal Processing Conference (EUSIPCO)*, Sept 2014, pp. 76–80.
- [10] X. Wu, N. C. Beaulieu, and D. Liu, "On favorable propagation in massive MIMO systems and different antenna configurations," *IEEE Access*, vol. 5, pp. 5578–5593, 2017.
- [11] M. Matthaiou, P. J. Smith, H. Q. Ngo, and H. Tataria, "Does massive MIMO fail in Ricean channels?," *IEEE Wireless Communications Letters*, vol. 8, no. 1, pp. 61–64, 2018.
- [12] V. Kolmonen, K. Haneda, T. Hult, J. Poutanen, F. Tufvesson, and P. Vainikainen, "Measurement-based evaluation of interlink correlation for indoor multiuser MIMO channels," vol. 9, pp. 311–314, 2010.
- [13] L. Liu, C. Oestges, J. Poutanen, K. Haneda, P. Vainikainen, F. Quitin, F. Tufvesson, and P. De Doncker, "The COST 2100 MIMO channel model," *IEEE Wireless Communications*, vol. 19, no. 6, pp. 92–99, 2012.
- [14] X. Gao, O. Edfors, F. Rusek, and F. Tufvesson, "Massive MIMO performance evaluation based on measured propagation data," vol. 14, no. 7, pp. 3899–3911, July 2015.
- [15] C.-M. Chen, A. P. Guevara, and S. Pollin, "Scaling up distributed massive MIMO: Why and how," in *2017 51st Asilomar Conference on Signals, Systems, and Computers*. IEEE, 2017, pp. 271–276.
- [16] Á. O. Martinez, J. ø. Nielsen, E. De Carvalho, and P. Popovski, "An experimental study of massive MIMO properties in 5G scenarios," vol. 66, no. 12, pp. 7206–7215, Dec 2018.
- [17] C. Shepard, J. Ding, R. E. Guerra, and L. Zhong, "Understanding real many-antenna MU-MIMO channels," in *2016 50th Asilomar Conference on Signals, Systems and Computers*, Nov 2016, pp. 461–467.
- [18] J. Flordelis, X. Gao, G. Dahman, F. Rusek, O. Edfors, and F. Tufvesson, "Spatial separation of closely-spaced users in measured massive multi-user MIMO channels," in *IEEE International Conf. on Commun. Citeseer*, 2015, pp. 1441–1446.
- [19] C. Masouros and M. Matthaiou, "Space-constrained massive MIMO: Hitting the wall of favorable propagation," *IEEE Communications Letters*, vol. 19, no. 5, pp. 771–774, 2015.
- [20] H. Yang and T. L. Marzetta, "Massive MIMO with max-min power control in line-of-sight propagation environment," *IEEE Transactions on Communications*, vol. 65, no. 11, pp. 4685–4693, Nov 2017.
- [21] "RENEW: Reconfigurable Eco-system for Next-generation End-to-end Wireless," <https://renew-wireless.org/>.
- [22] J. Hoydis, C. Hoek, T. Wild, and S. t. Brink, "Channel measurements for large antenna arrays," in *2012 International Symposium on Wireless Communication Systems (ISWCS)*. IEEE, 2012, pp. 811–815.
- [23] G. Caire, "On the ergodic rate lower bounds with applications to massive MIMO," vol. 17, no. 5, pp. 3258–3268, May 2018.
- [24] X. Du, Y. Sun, N. B. Shroff, and A. Sabharwal, "Balancing queuing and retransmission: Latency-optimal massive mimo design," *IEEE Transactions on Wireless Communications*, pp. 1–1, 2020.
- [25] Z. Jiang, A. F. Molisch, G. Caire, and Z. Niu, "Achievable Rates of FDD Massive MIMO Systems With Spatial Channel Correlation," vol. 14, no. 5, pp. 2868–2882, May 2015.
- [26] J. Choi, D. J. Love, and P. Bidigare, "Downlink Training Techniques for FDD Massive MIMO Systems: Open-Loop and Closed-Loop Training With Memory," *IEEE J. Select. Topics Signal Processing*, vol. 8, no. 5, pp. 802–814, Oct 2014.
- [27] M. Sadeghi, L. Sanguinetti, R. Couillet, and C. Yuen, "Large system analysis of power normalization techniques in massive MIMO," vol. 66, no. 10, pp. 9005–9017, 2017.
- [28] A. Adhikary, J. Nam, J. Y. Ahn, and G. Caire, "Joint spatial division and multiplexing: The large-scale array regime," vol. 59, no. 10, pp. 6441–6463, Oct 2013.
- [29] J. Hoydis, S. ten Brink, and M. Debbah, "Massive MIMO in the UL/DL of cellular networks: How many antennas do we need?," vol. 31, no. 2, pp. 160–171, February 2013.
- [30] E. Björnson, J. Hoydis, and L. Sanguinetti, "Massive MIMO has unlimited capacity," vol. 17, no. 1, pp. 574–590, 2017.
- [31] Junyoung Nam, Giuseppe Caire, Merouane Debbah, and H. Vincent Poor, "Capacity scaling of massive MIMO in strong spatial correlation regimes," 2018.
- [32] N. Fatema, G. Hua, Y. Xiang, D. Peng, and I. Natgunanathan, "Massive MIMO linear precoding: A survey," *IEEE Systems Journal*, vol. 12, no. 4, pp. 3920–3931, 2017.
- [33] Xiang Gao, Ove Edfors, Fredrik Rusek, and Fredrik Tufvesson, "Linear pre-coding performance in measured very-large MIMO channels," in *VTC Fall*, 2011, pp. 1–5.
- [34] 3GPP, "Study on 3D channel model for LTE," TS 36.873, 3rd Generation Partnership Project (3GPP), Mar. 2017.
- [35] X. Zhang, L. Zhong, and A. Sabharwal, "Directional training for fdd massive mimo," *IEEE Transactions on Wireless Communications*, vol. 17, no. 8, pp. 5183–5197, 2018.
- [36] Petr Beckmann, "Statistical distribution of the amplitude and phase of a multiply scattered field," *Journal of Research of the National Bureau of Standards*, 66D, vol. 3, pp. 231–240, 1962.
- [37] C. Shepard, H. Yu, N. Anand, E. Li, T. Marzetta, R. Yang, and L. Zhong, "Argos: Practical many-antenna base stations," in *Proc. of the 18th Annu. Int. Conf. on Mobile Computing and Networking*, New York, NY, USA, 2012, pp. 53–64, ACM.
- [38] "Google Map," <https://www.google.com/maps/@29.7200282,-95.3991931,88m/data=!3m1!1e3>, [Accessed July 7, 2019].
- [39] H. Krim and M. Viberg, "Two decades of array signal processing research: the parametric approach," vol. 13, no. 4, pp. 67–94, Jul 1996.
- [40] J. Kermoal, L. Schumacher, K. I. Pedersen, P. E. Mogensen, and F. Frederiksen, "A stochastic MIMO radio channel model with experimental validation," vol. 20, no. 6, pp. 1211–1226, 2002.
- [41] Vincenzo Lottici, Aldo D'Andrea, and Umberto Mengali, "Channel estimation for ultra-wideband communications," vol. 20, no. 9, pp. 1638–1645, 2002.
- [42] Nathaniel R Goodman, "Statistical analysis based on a certain multivariate complex Gaussian distribution (an introduction)," *The Annals of mathematical statistics*, vol. 34, no. 1, pp. 152–177, 1963.
- [43] Gene H Golub and Charles F Van Loan, *Matrix computations*, Johns Hopkins University Press, Baltimore, MD, USA, 2012.
- [44] P. Graczyk, G. Letac, and H. Massam, "The complex Wishart distribution and the symmetric group," *The Annals of Statistics*, vol. 31, no. 1, pp. 287–309, 2003.